scientific reports

Check for updates

OPEN

Colorimetric detection of edible oil oxidation using PAN–Congo red nanofiber mats

Ayat F. Hashim[1]✉, Hamdy A. Zahran[1], Sherine M. Afifi[1], Ahmed A. Abd-Rabou[2] & Said F. Hamed[1]

Lipid oxidation significantly compromises the safety, nutritional quality, and shelf life of edible oils, while conventional analytical methods are costly, time-consuming, and unsuitable for real-time monitoring. This study presents a novel nanofiber-based colorimetric sensor for rapid visual detection of lipid oxidation in soybean oil (SBO) and extra virgin olive oil (EVOO) under accelerated storage conditions (70 °C for 35 days). Polyacrylonitrile (PAN) nanofiber mats containing Congo red dye (CR, 0.0025%, 0.005%, and 0.01%, w/w) were fabricated via solution-blowing spinning and characterized using scanning electron microscopy (SEM) and Fourier transform infrared spectroscopy (FTIR). Oxidative deterioration was evaluated through conjugated diene (CD) and triene (CT) values, para-anisidine value (p-AnV), total polar compounds (TPC), volatile oxidation compounds, Rancimat induction period (IP), FTIR analysis, and cytotoxicity assays. Among the developed sensors, Mat_III (0.01% CR) exhibited the highest sensitivity, showing distinct color responses with ΔE values of 12.83 ± 0.20 in SBO and 9.83 ± 0.15 in EVOO, and rapid response times of 2.94 s and 4.71 s, respectively. After 35 days, CD, CT, and TPC increased to 3.83%, 0.96%, and 12.17% in SBO and 2.49%, 0.62%, and 7.83% in EVOO, while IP values decreased markedly, particularly in SBO, from 7.89 h to 2.04 h. Overall, these sensors offer a low-cost, rapid, and user-friendly approach for real-time oil oxidation monitoring.

Keywords Colorimetric sensor, Congo red, Nanofiber mats, Oil quality monitoring, Polyacrylonitrile

The quality of edible oils plays a vital role in food safety, nutritional value, and consumer acceptability. However, edible oils are highly prone to oxidation, leading to the formation of harmful compounds such as hydroperoxides, aldehydes, and ketones[1,2]. These oxidation products deteriorate oil quality, causing unpleasant odors, rancid flavors, and the generation of potentially toxic substances that may pose health risks[3]. Conventional analytical techniques, including peroxide value determination, spectroscopy, and gas chromatography, are commonly used to assess oil oxidation[4]. Although these methods are accurate and reliable, they often require skilled personnel, sophisticated instrumentation, and time-consuming procedures, limiting their suitability for rapid and on-site monitoring. Therefore, developing simple and real-time tools for monitoring lipid oxidation remains a critical need to improve oil shelf life and safety. Millions of tons of plastic are used annually in food packaging, with a significant portion ending up in landfills or oceans, causing environmental harm[5,6].

Recently, colorimetric sensors and nanofiber-based biosensors have gained increasing attention due to their high sensitivity, rapid response, and simple visual detection, making them suitable for applications in environmental monitoring, biomedical diagnostics, and industrial quality control[7–10]. Among these, nanofiber-based sensors have attracted considerable interest due to their high surface area, tunable functionality, and enhanced sensitivity. Such sensors have demonstrated promising applications in biomedical diagnostics, environmental monitoring, and food quality control. Over the past decade, solution-blow spinning has emerged as an efficient and scalable technique for nanofiber fabrication[11]. PAN, owing to its excellent mechanical strength, chemical stability, and processability, has been widely recognized as a suitable polymer for producing functional nanofiber mats[12,13].

CR is an azo dye known for its pH sensitivity and distinct colorimetric response under reactive environments, making it a promising candidate for sensing applications[14]. Previous studies have demonstrated the feasibility of CR-based sensors for oil oxidation detection, including CR-PAN nanofibers for sunflower oil oxidation, chitin-based CR sensors for aldehyde detection, and polyvinyl alcohol/Schiff fiber mats for visual oxidation

[1]Fats and Oils Department, National Research Centre, 33 El Bohouth St, Dokki, Giza 12622, Egypt. [2]Hormones Department, Medical Research and Clinical Studies Institute, National Research Centre, Cairo, Egypt. ✉email: af.hashim@nrc.sci.eg

assessment[15–17]. Despite these advances, existing studies remain limited in oil types, sensing performance comparison, and systematic correlation with comprehensive oxidation indices.

Accordingly, the present study addresses this gap by developing PAN/CR nanofiber mats as a simple, rapid, and cost-effective colorimetric sensor for visual detection of oxidation in SBO and EVOO. The study focuses on nanofiber fabrication, structural and morphological characterization, and evaluation of sensor performance across different oxidation levels using comprehensive physicochemical analyses, including conjugated diene and triene values, para-anisidine value, total polar compounds, volatile compounds, Rancimat test, and FTIR. The findings highlight the potential of PAN-CR nanofiber mats as practical tools for real-time oil oxidation monitoring.

Materials and methods

Materials

SBO and EVOO were purchased from the local Egyptian market. PAN (≥99%; average Mv 150000; CAS No: 25014-41-9), hydroxylamine hydrochloride (≥98%; CAS No: 5470-11-1), and a standard mixture of authentic fatty acids were obtained from Sigma-Aldrich (St. Louis, MO, USA). Dimethyl formamide (DMF) was purchased from Fine Chem. Ltd., Mumbai (India). CR (pH indicator, content (%) > 75%) was obtained from SD Fine Chem. Ltd., Mumbai (India). All other solvents and reagents were purchased from different suppliers. Normal skin fibroblasts (HSF) and normal kidney fibroblasts (BHK-21) were purchased from American Type Culture Collection (ATCC) and cultivated in RPMI 1640 complete medium supplemented with 10% heat-inactivated fetal bovine serum, 100 U/mL streptomycin, and 100 U/mL penicillin (Gibco, USA) at 37 °C in a humidified 5% CO_2 atmosphere.

Preparation and characterization of PAN-CR nanofiber mats

PAN nanofiber mats (Mat I–III) were developed via a solution-blowing spinning technology. Solution-blowing devices include an injection pump, a rotating nozzle, an air compressor-powered solution-blowing device, and a fiber collector. 15 g of PAN was dissolved in DMF to prepare the PAN solution. CR dye with various concentrations (0.0025, 0.005, and 0.01%) and 0.25 g of hydroxylamine hydrochloride were used. The mixture was stirred for 2 h at room temperature until it was completely homogenized. The solution-blowing spinning device was set as follows to generate the nanofiber mats: the mixture was pumped through a 23-gauge needle at an air pressure of 1% and a flow rate of 8 mL/h. The separation between the spinning nozzle and the nanofiber collector was set to 30 cm. The spinning needle was placed in the center of the concentric nozzle and extended 1 mm from it.

The FTIR spectra of the produced nanofiber mats were obtained with a resolution of 4000 –400 cm^{-1} using an FTIR Bruker Vertex 80v (National Research Centre, Egypt). The morphology of developed mats was shown using a scanning electron microscope (SEM, Quanta Fei 250, Republic Czech).

Evaluation of the effectiveness of PAN-CR nanofiber mats for the determination of oil oxidation

Oxidation of edible oils

Commercial SBO and EVOO were used in this study. The oil oxidation was accelerated using the Schall oven at 70 ± 2 °C for 35 days. Every 7 days, 20 mL of oil sample was taken from the bottle and stored immediately at − 20 °C for further analysis.

Evaluation of the oxidation state of edible oils

Edible oils undergo complex reactions that form different by-products such as CD, CT, TPC, and p-AV during the process of oxidation. Conjugated dienes and trienes are produced during the early stages of lipid oxidation, while p-AV, TPC, and volatile compounds are secondary oxidation products developed in later stages. Rancimat measurement is a thermal oxidative stabilityassay for edible oil.

Conjugated dienes and conjugated trienes determination Twenty milligrams of the oil sample were dissolved in 10 mL of n-hexane, and the absorbance was measured in the UV region using a UV–Vis spectrophotometer (T80 UV/VIS Spectrometer, PG Instruments Ltd., UK). Absorbance values at 232 and 268 nm were used to quantify CD and CT, respectively.

Total polar compounds determination The TestoTM instrument (Testo Inc. model 270, Pennsylvania, USA) was used to determine the TPC in oil samples according to[18]. This is a quick, on-site way to check for oil degradation that works by measuring the dielectric constant. When oils break down through oxidation and hydrolysis, non-polar triglycerides turn into polar compounds. This changes the oil's dielectric properties by raising its dielectric constant. The Testo tool uses a capacitive sensor to measure this change (from 0.0 to 40.0% TPM) and turns it into a percentage of TPC. When in use, the factory-calibrated probe is put directly into the hot oil (50 ± 1.0 °C), and within about 30 s, it gives a stable %TPC reading. A color-coded display often shows this reading right away so that the oil quality can be compared to regulatory limits (usually up to ~ 25% TPC).

Para-anisidine value determination The p-anisidine value was studiedto determinethe secondary oxidation products in oxidized oil samples[2]. 0.1 g of oil sample was weighed, and 5 mL of hexane was added. Absorbance against hexane at 350 nm was recorded (A1). A mass of 0.1 g of oil sample was weighed, 5 mL of hexane was added, and 1 mL of 2.5 g/L P-AV solution was added. It was kept in the dark for 10 min. Absorbance was recorded at 350 nm against the reagent blank (A2). P-AV was calculated according to the following equation:

$$p - AV = \frac{5\ X\ (1.2\ X\ (A2 - A1))}{g\ (oil)}$$

Volatile compounds The volatile compounds released from the oxidized oils as secondary oxidation products were measured in the headspace using an HP-5MS fused silica capillary column (30 m, 0.25 mm i.d., 0.25 mm film thickness), a gas chromatograph (Agilent 8890 GC System), and a mass spectrometer (Agilent 5977B GC/MSD)[14]. Oxidized oils (5 mL) were shaken in a 20 mL vial for 10 min at 45 °C before investigation.

Rancimat measurement 3 g of the oil sample was taken to determinethe thermal oxidative stability via Rancimat equipment (Model 892 Professional Rancimat, Metrohm SA, Herisau, Switzerland) with 20 L/h airflow rate at 110 °C. The oil oxidative stability was examinedover the time corresponding to the induction period.

Response of PAN-CR nanofiber mats to oxidized oils

The aluminum foil-covered nanofiber mats were cut into circles and placed within the vial with the cap, ensuring they did not touch the oil samples. The oxidized oil sample (5 g) was taken and put inside a sealed vial (20 mL) after each time to measure the response time. All changes in mat color were measured after 3 min to standardize the exposure time. The color variation (ΔE) between the nanofiber mats before and after being exposed to oxidized oil samples was determined by the colorimeter (CR-10, Konica Minolta Sensing, Inc., Sakai, Osaka, Japan). For the control sample, the nanofiber mats were placed in an empty 20 mL vial. The ΔE was calculated after the color parameters L^* (lightness), a^* (red-green), and b^* (yellow-blue) were measuredusing the following equation:

$$\Delta\ \mathbf{E} = \sqrt[2]{(\Delta\ \mathbf{L}^*)^2 + (\Delta\ \mathbf{a}^*)^2 + (\Delta\ \mathbf{b}^*)^2}$$

$\Delta L^* = L^* - L^{0*}$, $\Delta a^* = a^* - a^{0*}$, and $\Delta b^* = b^* - b^{0*}$ are defined. The nanofiber mats had the color values L^0, a^0, and b^0 before the exposure to oxidized oil, and L^*, a^*, and b^* following the exposure.

Cytotoxicity experiment

The cytotoxicity experiments were performed using the direct contact method according to the previously reported method[19], with some modifications. The safety of the developedfibers (MAT_I-III) against the two normal cell lines (HSF and BHK-21) was investigated using an MTT assay. Concisely, a 96-well tissue culture plate was inoculated with 1×10^5 cells / well and incubated at 37 °C for 24 h to grow to subconfluency (about 80% confluent). Cells were washed 3 times, and then the developed fibers (MAT_I-III) were placed directly on the cells. For the positive control sample, a piece of sterile filter paper was saturated with doxorubicin (DOX), and the filter paper was placed directly on the cells. Further, 150 µL of complete medium was deposited over the samples. After that, plates were incubated at 37 °C for 0, 1 h, 2 h, 4 h, 8 h, 12 h, and 24 h and examined. MTT solution was prepared (5 mg/mL in PBS) (BIO BASIC CANADA INC), and 20 µL MTT solution was added to each well. The plate was shaken at 150 rpm for 5 min to thoroughly mix the MTT into the media. The mixture was incubated at 37 °C for 4 h to allow the MTT to be metabolized. After incubation, the medium was carefully removed and 200 µL DMSO was added to resuspendformazan. The optical density was obtained at 450 nm, and the background was subtracted at 620 nm. The HSF and BHK-21cell viability % were measured.

Statistical analysis

Statistical differences were evaluated using one-way analysis of variance (ANOVA) followed by Duncan's new multiple range test at $p < 0.05$, performed with Statistica 6 software (StatSoft Inc., Tulsa, OK, USA). Results are expressed as the mean ± standard deviation of three independent replicates, and error bars are shown in the figures.

Results and discussion

Effect of CR concentration on the morphology of PAN nanofiber mats

The surface morphology of the electrospun nanofiber mats containing different concentrations of CR was examined by scanning electron microscopy, as shown in Fig. 1. All samples exhibit a continuous fibrous network without bead formation, indicating stable electrospinning conditions. As shown in Fig. 1A, nanofiber mats containing 0.0025% CR consist of long, predominantly straight fibers with slight curvatures. The fibers display a relatively smooth surface with minor surface irregularities, which may be attributed to solvent evaporation during electrospinning. The nanofibers are loosely packed, resulting in a low-density and more open fibrous structure. Increasing the CR concentration to 0.005% (Fig. 1B) leads to noticeable changes in morphology. The fibers remain continuous and smooth; however, more pronounced bending and waviness are observed compared to Fig. 1A. The fiber network becomes moderately denser, suggesting enhanced intermolecular interactions between PAN and CR molecules during fiber formation.

At the highest CR concentration (0.01%), Fig. 1C reveals a clear increase in fiber curvature, looping, and entanglement, resulting in a more compact and densely packed nanofibrous mat. The higher degree of fiber interconnection indicates increased solution conductivity and viscosity caused by the higher CR content, which influences jet stretching and fiber deposition behavior. Quantitative analysis shows that the average fiber diameters increase gradually from 286 nm (MAT-I) to 305 nm (MAT-II) and 315 nm (MAT-III), confirming that CR concentration has a measurable effect on fiber thickness. The intermediate morphology observed in Fig. 1B supports this progressive trend in both fiber diameter and structural complexity. These observations

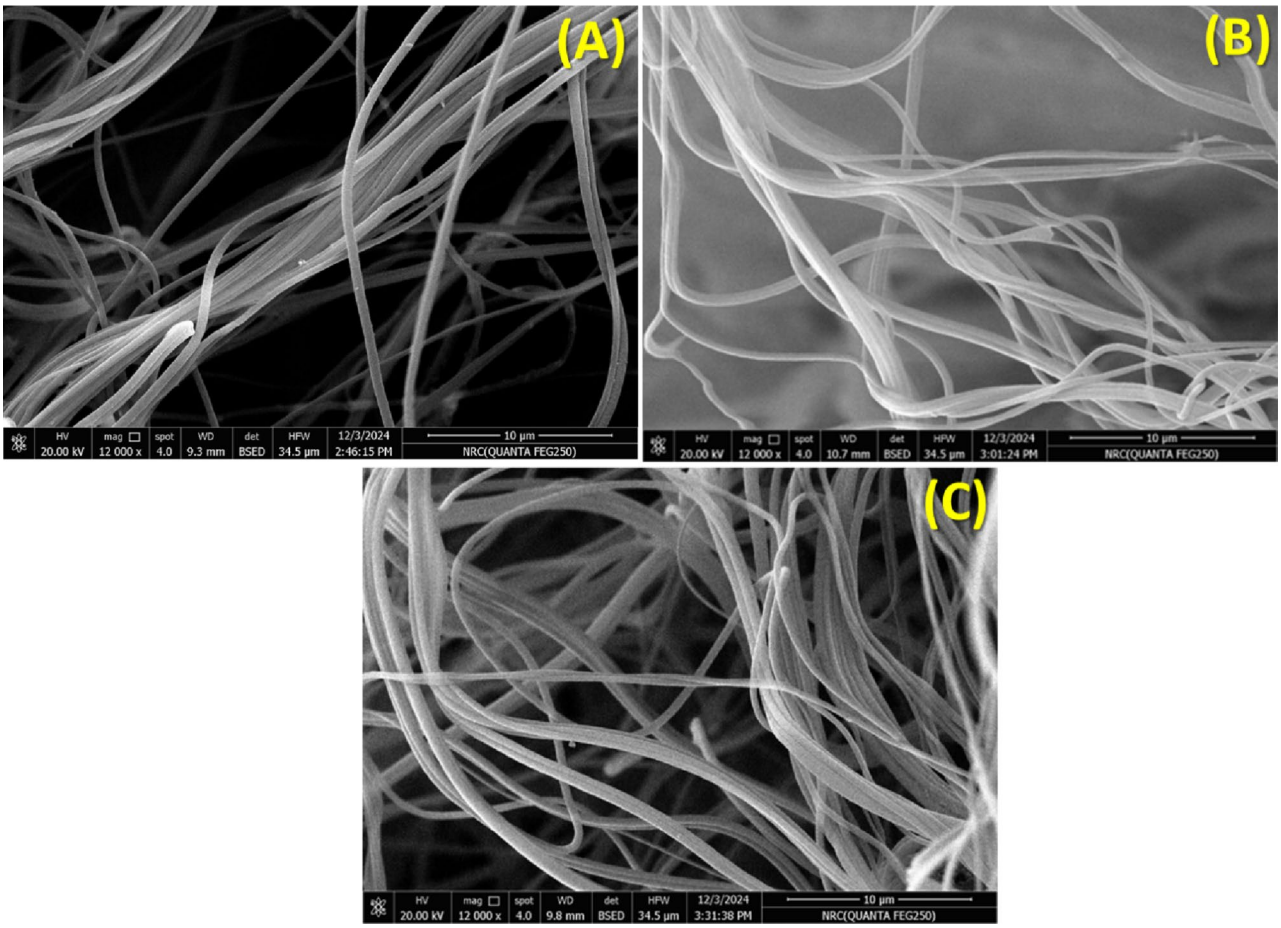

Fig. 1. SEM micrographs of CR-PAN nanofiber mats (**A**) nanofiber mat with 0.0025% CR, (**B**) nanofiber mat with 0.005% CR, and (**C**) nanofiber mat with 0.01% CR.

are consistent with previous reports. It was reported that smooth and uniform nanofiber surfaces in CR-loaded nanofiber mats[17], while it was demonstrated that dye incorporation into PAN nanofibers can significantly alter fiber diameter, curvature, and packing density[20].

FTIR analysis

The FTIR spectra of the electrospun nanofiber mats (MAT_I–MAT_III) containing different concentrations of CR are presented in Fig. 2, recorded over the wavenumber range of 500–4000 cm^{-1}. The spectra were analyzed to elucidate chemical interactions and structural modifications resulting from CR incorporation into the polymer matrix[21]. MAT_I exhibits the characteristic absorption bands of the polymer matrix, including a broad band around ~ 3500 cm^{-1} corresponding to overlapping O–H and N–H stretching vibrations, and C–H stretching vibrations near ~ 3000 cm^{-1}. The strong absorption band observed around ~ 2240 cm^{-1} is attributed to the nitrile (C ≡ N) stretching vibration of PAN, confirming the preservation of the polymer backbone[22].

Upon increasing the CR concentration in MAT_II and MAT_III, noticeable spectral changes are observed. The O–H/N–H stretching band becomes broader and shifts toward lower wavenumbers, indicating the formation of stronger hydrogen-bonding interactions between the sulfonic and azo groups of CR and the polar functional groups of PAN. This red shift suggests enhanced intermolecular interactions as CR content increases. Additionally, the absorption intensity in the 1500–1000 cm^{-1} region increases progressively from MAT_I to MAT_III. These bands are associated with aromatic C = C stretching and azo (–N = N–) vibrations originating from CR, confirming successful dye incorporation into the nanofiber matrix. The enhanced intensity of these peaks in MAT_III reflects the higher CR loading and stronger CR–PAN interactions.

The most pronounced spectral changes in MAT_III indicate increased molecular interactions and possible dye aggregation at higher CR concentrations, which may influence both fiber morphology and sensing performance. Similar CR-induced spectral shifts and interaction mechanisms were previously reported by[17], demonstrating the effect of dye concentration on polymer–dye interactions in nanofibrous systems. Overall, the FTIR results confirm effective CR incorporation into the nanofiber mats and reveal that hydrogen bonding and aromatic–polymer interactions are the dominant mechanisms governing structural modification within the nanofiber matrix.

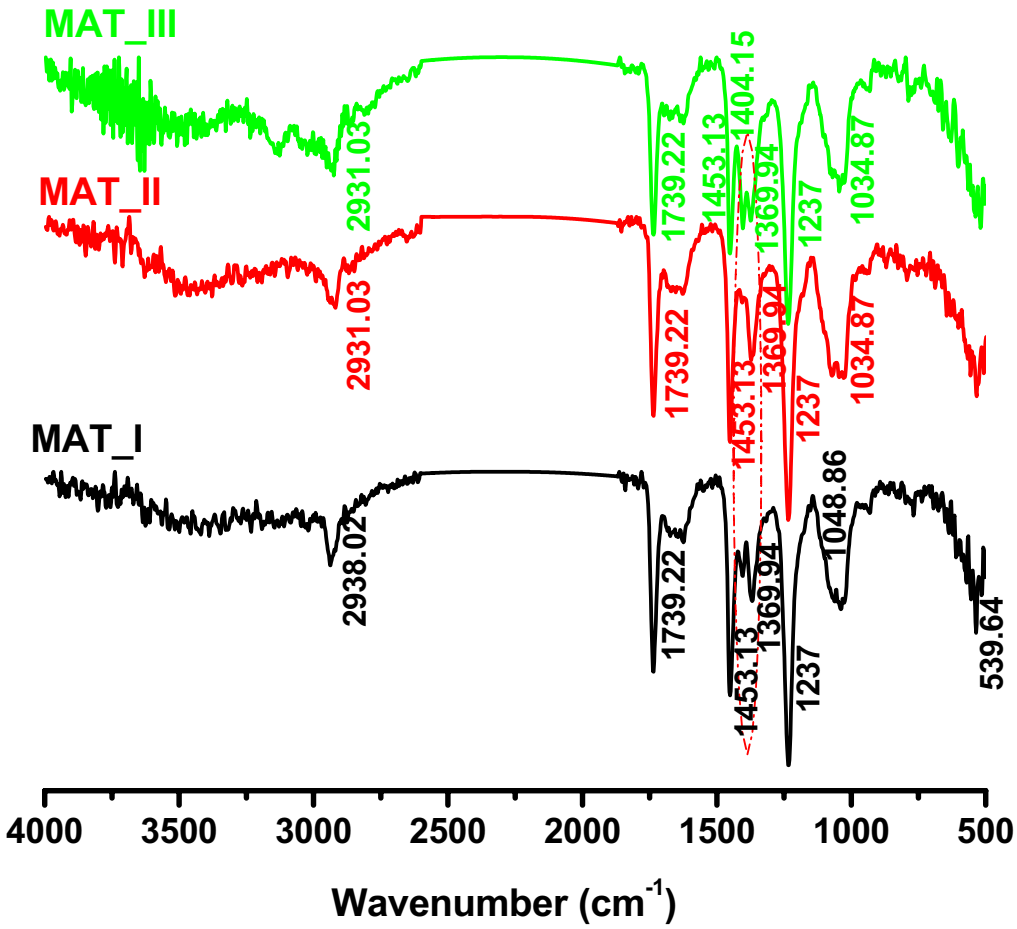

Fig. 2. PAN nanofiber mats with various concentrations of CR.

Oxidative stability

The variation in fatty acid compositions and natural antioxidants in edible oils is a primary cause of the differing oxidation rates[23–25]. The formation of CD, (CT), (p-AV), TPC, volatile compounds, and IP (Rancimat assay) over time was studied to assess the oxidation levels in both oils subjected to heating at 70 °C ± 2 for 35 days. These parameters are critical points that determine the quality, shelf life, and nutritional value of edible oils.

Conjugated dienes and trienes

CD and CT are commonly used to measure the rate of oxidation in edible oils. Conjugated dienes and trienes can be assessed by monitoring their absorbance at 232 nm (K_{232}) and 268 nm (K_{268}), respectively. In general, decreased oxidation stability of vegetable oils is indicated by more conjugated dienes and triene values[26]. The conjugated diene and conjugated triene content rose because of the high concentration of main lipid oxidation products. However, their reduction was linked to the breakdown of major lipid oxidation products during heating. The CD amount is significant for primary oxidation, while the CT incidence is caused by the formation of oxidation by-products such as unsaturated α- and β-diketones or β-ketones[27].

The CD content was slightly higher in fresh SBO (0.16%) than in EVOO (0.13%), as displayed in Table 1. These values rose to 3.83% in SBO and 2.49% in EVOO by day 35. The faster increasein dienes in SBO reflected its lower oxidative stability. Initially, both oils had a triene content of 0.06%. However, triene levels increasedas oxidation progressed to 0.96% in SBO and 0.62% in EVOO by day 35. The higher increase in diene and triene contents in SBO proposed a more oxidative breakdown of its higher content of polyunsaturated fatty acids (linoleic and linolenic acids). According to the International Olive Council, CD and CT for edible EVOO should not exceed the maximum limit of 2.50 and 0.22, respectively[28,29].

Total polar compounds and para-ansidine value

The TPC determines the breakdown products (e.g., free fatty acids, polymerized compounds, and oxidized triglycerides) generated when edible oils are oxidized. High values of total polar compounds show deteriorated oil quality and a potential health risk. The TPC values were 0.50% in fresh oils. Total polar compounds increased dramatically to 12.17% in SBO and 7.83% in EVOO at day 35. The oil oxidation is directly linked to the rise in total polar compounds. The higher amounts in SBO show that it is more prone to oxidation. The results indicate that EVOO exceeds SBO in stability over time. It indicated that the high oleic acid content and the

Days	SBO	EVOO	SBO	EVOO	SBO	EVOO	SBO	EVOO
	CD (%)		CT (%)		TPC (%)		*p*-AV	
Fresh	0.16 ± 0.01	0.13 ± 0.01	0.06 ± 0.01	0.06 ± 0.02	0.50 ± 0.00	0.50 ± 0.00	3.96 ± 0.01	3.89 ± 0.01
7	2.17 ± 0.11	1.54 ± 0.03	0.54 ± 0.03	0.43 ± 0.01	6.83 ± 0.29	5.00 ± 0.00	4.31 ± 0.03	4.01 ± 0.05
14	2.44 ± 0.04	1.85 ± 0.11	0.61 ± 0.01	0.46 ± 0.03	7.67 ± 0.29	5.67 ± 0.29	4.32 ± 0.025	5.97 ± 0.015
21	2.65 ± 0.11	1.83 ± 0.14	0.66 ± 0.03	0.49 ± 0.01	8.33 ± 0.29	6.00 ± 0.00	5.16 ± 0.01	6.48 ± 0.01
28	3.24 ± 0.04	2.17 ± 0.11	0.78 ± 0.03	0.54 ± 0.03	9.67 ± 0.29	6.67 ± 0.29	5.49 ± 0.05	11.75 ± 0.029
35	3.83 ± 0.04	2.49 ± 0.11	0.96 ± 0.00	0.62 ± 0.03	12.17 ± 0.29	7.83 ± 0.29	9.19 ± 0.029	12.21 ± 0.011

Table 1. Changes in conjugated diene, conjugated triene, total polar compound, and p-anisidine value in SBO and EVOO during storage. Data were expressed as the mean of three replicates ± SD.

Compounds	7 days		14 days		21 days		28 days		35 days	
	SBO	EVOO	SBO	EVOO	SBO	EVOO	SBO	EVOO	SBO	EVOO
n-Hexylmethyl amine	62.69 ± 0.15	7.52 ± 0.05	83.94 ± 0.14	53.4 ± 0.017	87.75 ± 0.055	78.73 ± 0.2	89.13 ± 0.035	85.53 ± 0.01	91.57 ± 0.015	80.47 ± 0.11
Pentanal	4 ± 0.11	-	5.56 ± 0.035	-	8.35 ± 0.1	5.79 ± 0.017	15.45 ± 0.01	9.12 ± 0.05	27.32 ± 0.15	10.01 ± 0.3
Hexanal	6.87 ± 0.3	3.56 ± 0.2	9.52 ± 0.055	6.66 ± 0.015	10.41 ± 0.0	7.79 ± 0.11	19.24 ± 0.015	8.26 ± 0.2	19.6 ± 0.015	15.32 ± 0.035

Table 2. Changes in main volatile compounds in SBO and EVOO during heating time for 35 days. Data were expressed as the mean of three replicates ± SD.

antioxidant compounds present in EVOO successfully delay the oxidation of lipids. Dienes, trienes, and total polar compounds increased more quickly in SBO, suggesting that they are more susceptible to oxidation (Table 1). These results are consistent with[30], who showed that the high content of monounsaturated fatty acids in olive oil and the antioxidant profile gave greater oxidative stability.

p-AV is a method for measuring secondary oxidation products such as aldehydes[17]. Aldehydes are the carbonyl compounds formed by the decomposition of hydroperoxides. It can be used as a marker to determine the degradation of peroxidized materials produced by the heating process. According to[31], the breakdown of oil hydroperoxides caused the p-AV of heated sunflower oil to rise with increasing heating time, which is in agreement with our results presented in Table 1.

Volatile compounds analysis

Advanced gas and nanostructured sensors have been successfully applied for the detection of volatile organic compounds, including amines and pyridine derivatives, demonstrating high sensitivity and selectivity[32–35]. These approaches highlight the potential of nanofiber- and polymer-based sensors for monitoring volatile products generated during oil oxidation. Table 2 displays the presence of various volatile chemical compounds in SBO and EVOO over different intervals during heating at 70 ± 2 °C. The main compounds recognized include n-hexylmethylamine, pentanal, and hexanal. The concentration of N-hexylmethylamine varies significantly over time. Its concentration was 62.69% and 89.13% in SBO at 7 and 35 days, respectively. The same trend was observed in EVOO, rising from 7.52% to 80.47%. This increase suggests potential oxidation-related deterioration or reactivity with other components over time[20].

Pentanal and hexanal, the dominant aldehydes in this study are commonly related to lipid oxidation, reducing the stability and quality of oil[36]. The two oils had similar trends, though SBO showed higher n-hexylmethylamine and less aldehyde than EVOO. This might be related to differences in antioxidant capacity and the fatty acid composition of the two oils[20]. Hexanal was present at higher levels in SBO due to hydrolysis reactions. These results support that oxidation and hydrolysis reactions contribute notably to the chemical changes of these oils over time. While SBO breaks down more quickly because of its higher aldehyde generation, EVOO was stable for a longer time because of a different oxidative pathway. The antioxidant properties play a crucial role in extending the shelf life of oils and other lipid-based products. By effectively scavenging free radicals and inhibiting oxidative reactions, these antioxidants prevent the formation of off-flavors, rancidity, and nutrient loss, which are common indicators of product deterioration[37,38]. These findings align with previous research on the kinetics of edible oil lipid oxidation[39].

Rancimat measurement

The IP is a vital indicator for evaluating the oxidative stability of edible oils, which directly impacts their quality and shelf life. Our results (Fig. 3A & B) reveal that EVOO constantly demonstrated a longer IP than SBO across all heating intervals. SBO had an IP of 7.89 h, while fresh EVOO showed an IP of 8.61 h. The oxidative stability of both oils decreased over time, though at different rates. By day 35, the IP for SBO had sharply declined to 2.04 h, whereas the IP for EVOO had fallen to 4.98 h. This significant difference indicates that EVOO is more resistant to oxidation than SBO.

The two oils have various levels of oxidative stability because of their different compositions. EVOO is rich in monounsaturated fatty acids, and it also has higher levels of natural antioxidants such as tocopherols and

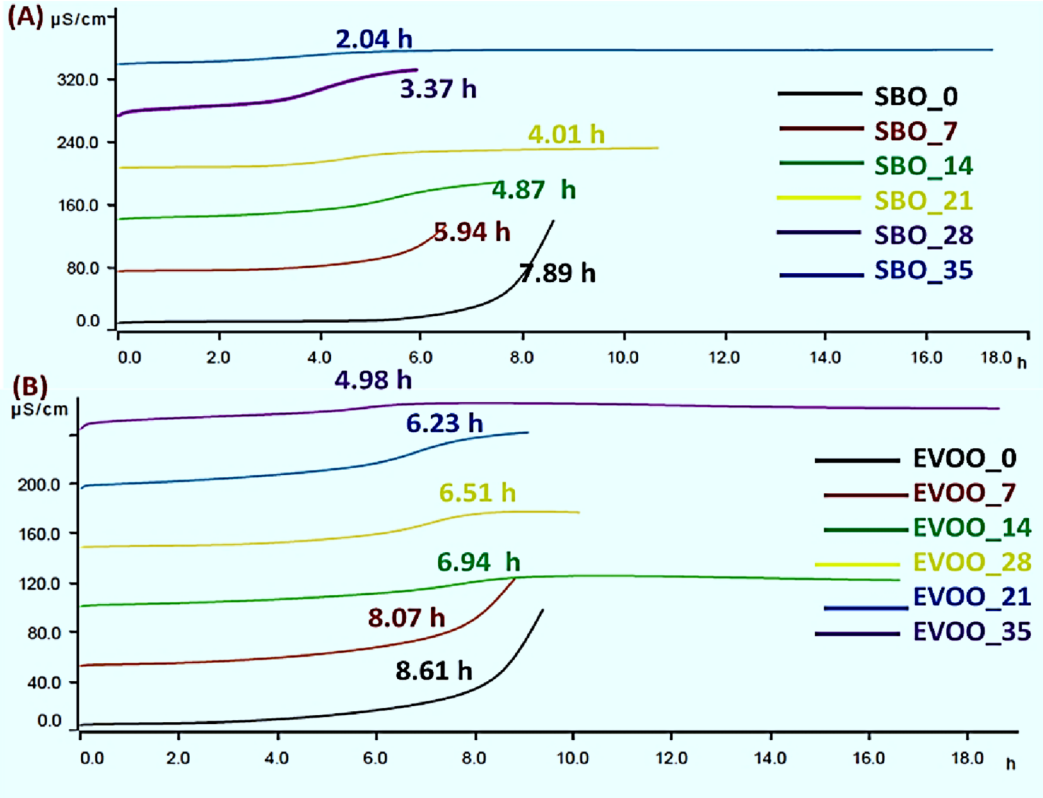

Fig. 3. The induction period declines over time for SBO and EVOO.

polyphenols[40]. These compounds are crucial for delaying lipid oxidation, which extends the induction period. Conversely, SBO has a high content of polyunsaturated fatty acids, which can be more easily oxidized and cause a quick drop in stability[41].

FTIR measurements

FTIR spectra (Fig. 4A-F) revealed the structural changes in SBO and EVOO during heating time at 60 °C. The FTIR spectra of the oil samples showed distinct absorption bands linked to oil oxidation compounds. When C-O stretching vibrations caused a broad absorption band in the 1000–1300 cm^{-1} range, it indicated the ester bond formation, whichis characteristic of polymerization products[42]. This aligns with the increase of polymers and high-molecular-weight molecules during the later stages of oil oxidation[43]. The FTIR spectra of SBO demonstrated significant variations with heating time, which indicated oil oxidation. The intensity of the carbonyl stretching peak at 1743 cm^{-1} increased from fresh to oxidized oil at day 35, indicating the oxidation products such as aldehydes, ketones, and carboxylic acids. Furthermore, a slight decrease in intensity of the peak C-H stretching peak at 3008 $cm^{-1}$is associated with unsaturated fatty acids, indicating the double bond breakdown due to the oxidation process[44]. These alterations, in general, proposed that SBO had extensive oxidation over time. FTIR spectra of EVOO also demonstrated signs of oxidation, but the changes are less pronounced compared to SBO.

The peak at 1743 cm^{-1}increases in intensity from EVOO_0 to EVOO_35, representing the carbonyl compound formation due to oxidation. Conversely, the increase is less significant than in SBO. The peak at 3008 cm^{-1} shows the least change, suggesting that the breakdown of unsaturated bonds is less severe in EVOO. The hydroxyl region also displayed less change compared to SBO, representing a lower hydroperoxide formation. In general, EVOO exhibits signs of oxidation, but the extent is milder than that of SBO. SBO showed more noticeable oxidation levels than EVOO. The carbonyl peak was increased and was highly distinct in SBO, which might be due to a large development of oxidation products. Furthermore, SBO revealed a more pronounced decline in the C-H stretching peak, demonstrating a high degree of unsaturated bond. The more noticeable changes in the hydroxyl area also indicate increased hydroperoxide production. However, in these regions, EVOO displayed less harsh oxidation, suggesting a slower process. SBO oxidizes higher than EVOO, according to the FTIR data. These findings are consistent with previous research on the oxidative deterioration of oils. An alteration in absorbance at 3009 $cm^{-1}$and 722 cm^{-1} was detected because of the oxidation of SBO, which made a loss of the cis-disubstituted olefin groups[45]. In addition, it was determined that fluctuations at 1157 cm^{-1} and 1745 cm^{-1} corresponded to the breakdown of hydroperoxide in soybean and sunflower oils after deep-frying chickpea splits for an extended period[46]. FTIR spectra at 3750–3150 cm^{-1} of unoxidized and oxidized soybean and sunflower oils were studied[47].

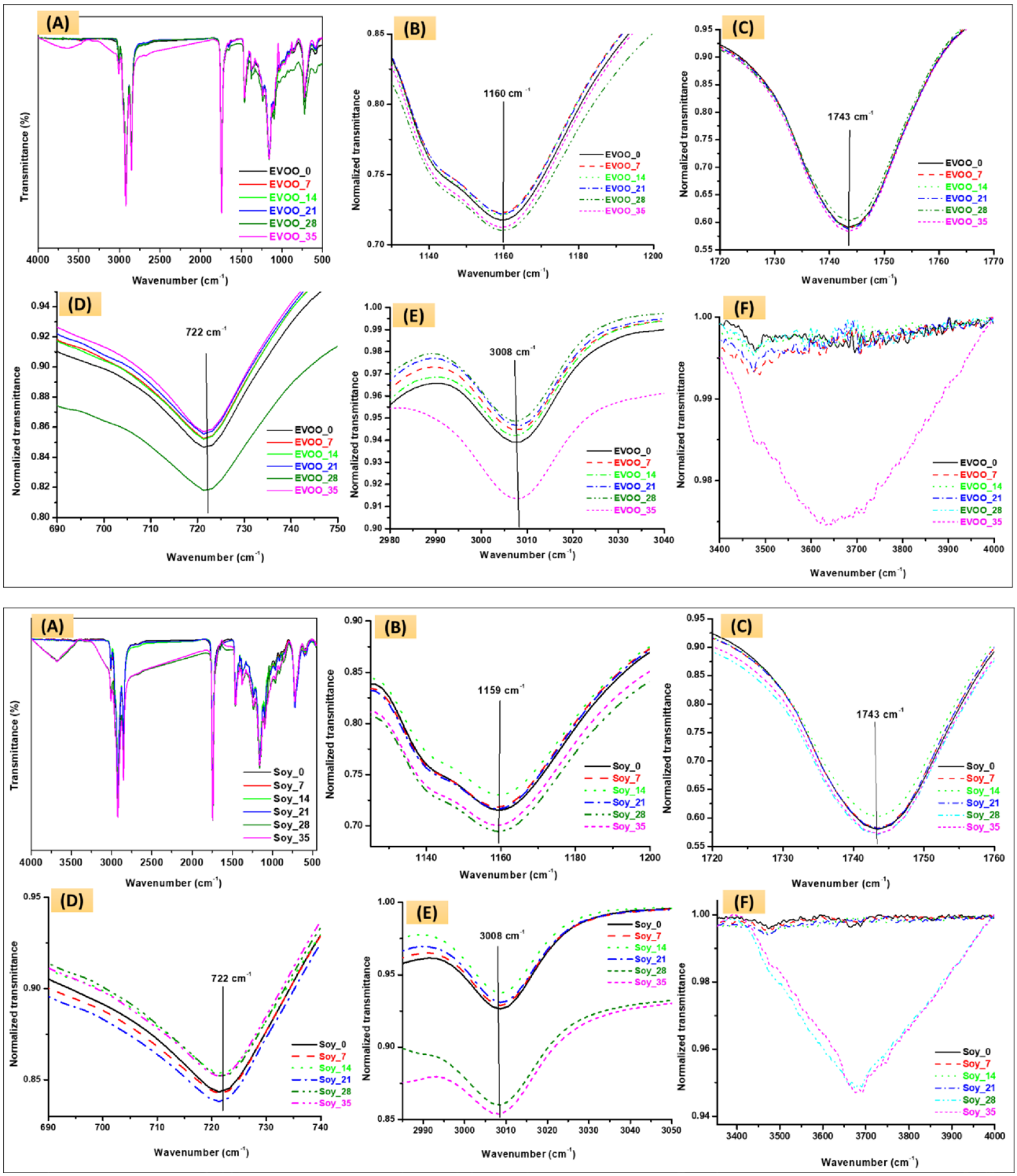

Fig. 4. FTIR spectra of (**A**) fresh and oxidized SBO and EVOO, spectral changes due to the development of secondary oxidation products (aldehydes, and ketones) at (**B**) 1160 cm^{-1}, and (**C**) 1743 cm^{-1}; a reduction in unsaturated fatty acid amounts at (**D**) 722 cm^{-1}, (**E**) 3008 cm^{-1}; and formation of hydroperoxides (**F**) 3400–3600 cm^{-1}.

Effectiveness of nanofiber mat for SBO and EVOO oxidation detection

Color variation (ΔE) was utilized to track visual changes in SBO and EVOO over 35 days of storage. Figure 5A showed that the ΔE of both oils increased over time due to oxidation products. SBO showed a significant increase in ΔE, reaching approximately 13.0 by the end of the storage period. While EVOO increased slowly, reaching approximately 6.5 by day 35. EVOO has excellent oxidative stability due to its high content of naturally occurring

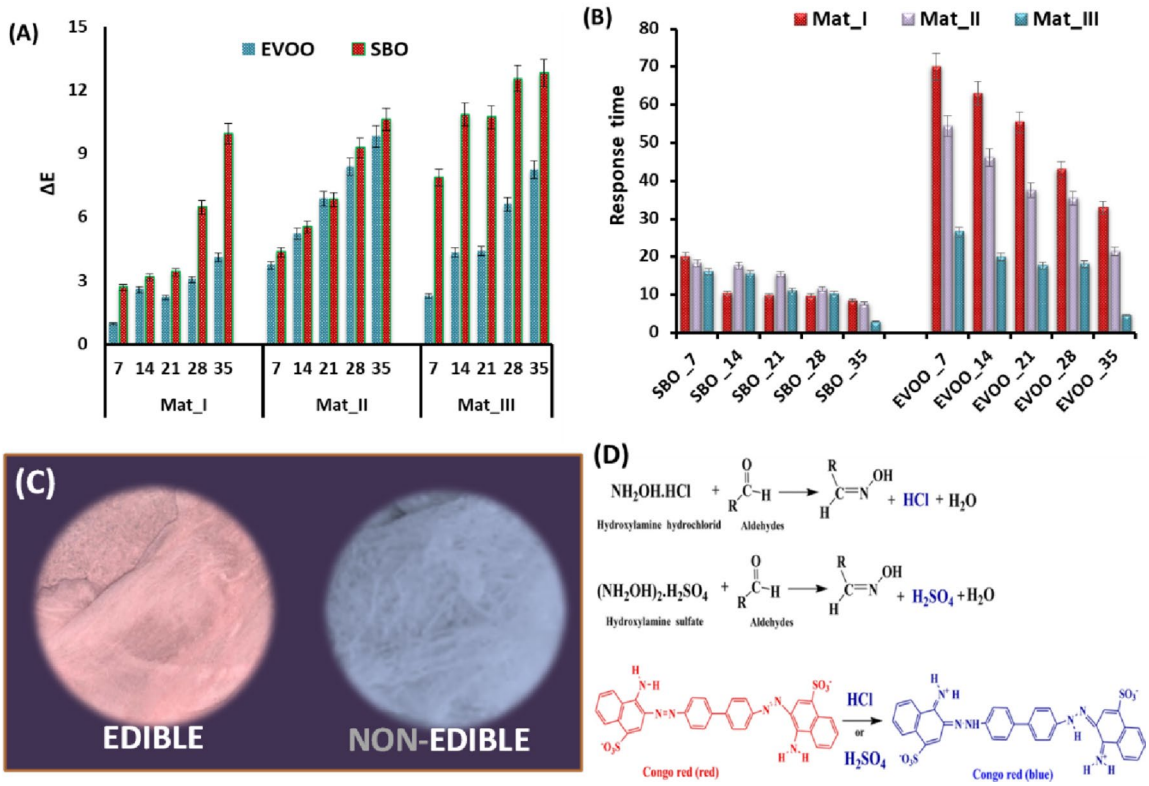

Fig. 5. (**A**) color change (ΔE) (**B**) response time of the effectiveness of nanofiber mats to oxidized oils; (**C**) visual color change before and after exposure to oxidized SBO for edibility detection, and (**D**) sensing mechanism of colorimetric sensor to volatile compounds (Hashim et al., 2025).

antioxidants such as tocopherols and phenolics[48]. However, because SBO contains high polyunsaturated fatty acid content, particularly linoleic and Linolenic acids, it degrades more quickly during oxidation, producing secondary oxidation products such as acids and aldehydes that change the color of the nanofiber mats. Colorimetric approaches are effective at detecting degradation in oil quality, as seen by increasing ΔE values.

The ΔE of nanofiber matvalues showed more change with higher dye concentrations during the storage time. Mat_III constantly demonstrated higher ΔE values than Mat_I and Mat_II when exposed to the oxidized oils. This implies that mats with a higher CR load not only detect changes faster but also display greater visual differentiation. Consequently, it made them easier to interpret both instrumentally and by the naked eye. The great change in ΔE with increasing dye load can be clarified by the higher number of dye molecules available to undergo structural or electronic transitions (e.g., protonation or binding with oxidation products), which strengthens the apparent color change[49]. It also indicated high dye load mats, making them more suitable for early detection applications, especially in more oxidation-prone oils like SBO[50].

CR was incorporated with increasing concentrations into Mat_I, Mat_II, and Mat_III sensor mats to study the effect of dye loading on colorimetric sensitivity and detection performance. Mat_III with the highest dye concentration demonstrated the fastest response time (2.94 s for SBO and 4.71s for EVOO by 35 days) due to a fast visual response upon exposure to volatile compounds (Fig. 5B). Mat_II demonstrated an intermediate response time. Mat_I, with the lowest dye concentration, had the slowest response, probably due to fewer reactive sites available for identifying acidic and aldehydic degradation compounds. These findings highlighted that increasing the dye concentration improved the sensitivity of mats and accelerated color change[51]. The influence of CR concentration on response time and ΔE supported the possibility of modifying sensor performance by adjusting dye loading. For commercial or consumer use, sensor mats with higher dye content (e.g., Mat_III) could present more sensitive and visually obvious indicators of oil oxidation (Fig. 5C).

The applicability of PAN–Congo Red nanofiber mats for edible oil oxidation monitoring depends on their stability and performance under real food conditions, where oils are subjected to variable temperature, light, oxygen, moisture, and matrix interactions (Fig. 5D). Although PAN provides good structural and chemical stability, prolonged heat and light exposure may cause polymer aging or dye leaching, leading to signal drift. In real oils, differences in fatty acid composition, antioxidants, and minor components can alter oxidation behavior and interfere with the colorimetric response. Therefore, despite promising laboratory results, ensuring reliable performance under long-term storage and repeated heating requires improved dye stabilization and oil-specific calibration.

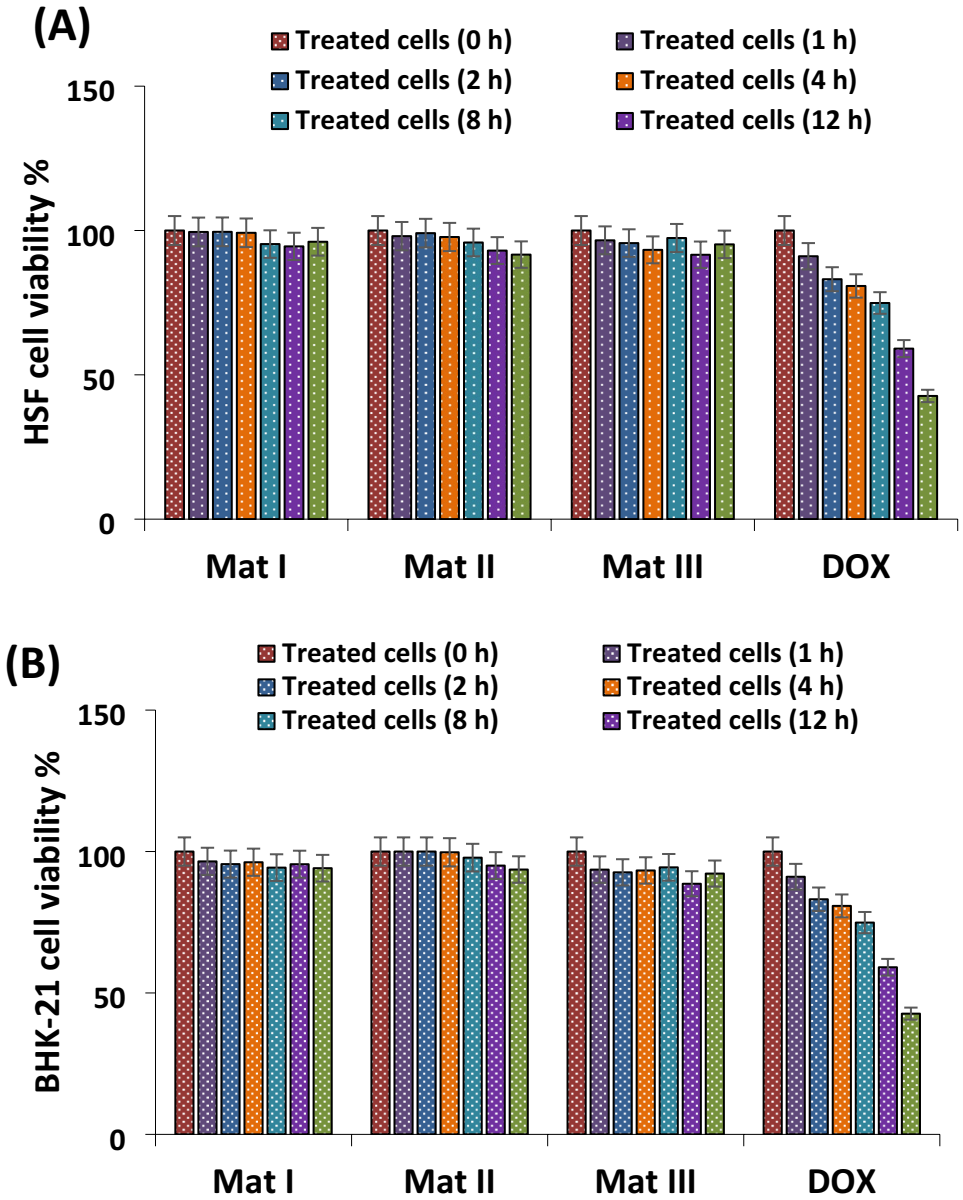

Fig. 6. Safety profile of fibers (I-III) and DOX against (**A**) normal skin HSF cells and (**B**) normal kidney BHK-21 over 0 h, 1 h, 2 h, 4 h, 8 h, 12 h, and 24 h ($n = 3$).

Sensor safety

Safety against normal skin cells

The current study demonstrated that all developed nanofiber mats (I-III) were safe against the human skin fibroblast (HSF) normal cells over 24 h (Fig. 6A). The HSF cell viability was 99.5% after 1 h incubation with Mat I, then slightly decreased to be 94.5% after 12 h and slightly increased after 24 h incubation to be 96.1%. The HSF cell viability was 98.04% after 1 h incubation with Mat II, then decreased to 93.1% after 12 h and slightly decreased after 24 h incubation to 91.6%. The HSF cell viability was 96.6% after 1 h incubation with fiber III, then decreased to 91.5% after 12 h, and increased after 24 h incubation to 95.2%. DOX, as a positive control, recorded 91.08% HSF cell viability after 1 h incubation then significantly decreased to 59.1% and 42.6% after 12 h and 24 h, respectively (Fig. 6A). These results are consistent with a previous study suggested that if the used materials are composed of PAN, they do not pose a safety risk to the consumer[52].

Safety against normal kidney cells

The current study demonstrated that all producednanofiber mats (I-III) were safe against the Baby Hamster Kidney fibroblasts (BHK-21 cells) over 24 h (Fig. 6B). The BHK-21 cell viability was 96.5% after 1 h incubation with Mat I, then slightly decreased to be 95.5% after 12 h and slightly decreased after 24 h incubation to be 94.1%. The BHK-21 cell viability was 100% after 1 h incubation with Mat II, then decreased to 95.05% after 12 h and slightly decreased after 24 h incubation to 93.6%. The BHK-21 cell viability was 93.6% after 1 h

incubation with Mat III, then decreased to 88.6% after 12 h and increased after 24 h incubation to 92.3%.DOX, as a positivecontrol, recorded 90.2% BHK-21 cell viability after 1 h incubation then significantly decreased to 57.2% and 34.8% after 12 h and 24 h, respectively (Fig. 6B). All these observations are in parallel with a previous study indicating that PAN fibers are safe to be used in fruit and vegetable food packaging materials, which need long-term storage and transportation[53].

Conclusion

In this study, PAN nanofiber mats incorporated with varying concentrations of CR were successfully fabricated and evaluated as colorimetric indicators for monitoring oil oxidation. FTIR analysis confirmed the presence of hydrogen-bonding interactions between the functional groups of PAN and CR molecules, which became more pronounced at higher dye concentrations, indicating effective dye incorporation and strong polymer–dye interactions. The oxidative stability assessment revealed that EVOO exhibited a longer induction period than soybean oil, confirming its superior oxidation resistance. Among the developed systems, MAT_III demonstrated the highest sensitivity, as evidenced by the largest color difference (ΔE) values and the fastest response to oxidized oils. Furthermore, cytotoxicity assays confirmed that all nanofiber mats were non-toxic toward HSF and BHK-21 cells after 24 h exposure, highlighting their potential safety for food-related applications.

From a translational perspective, these findings suggest that CR-loaded PAN nanofiber mats represent a promising platform for intelligent food packaging applications aimed at real-time oil quality monitoring. However, several challenges must be addressed before commercialization. Key knowledge gaps include long-term stability of the dye under varying storage and processing conditions, potential dye migration into food matrices, and the durability of sensor performance during extended shelf life. Future studies should therefore focus on comprehensive preclinical evaluations, including overall and specific migration tests, advanced toxicological assessments, sensory impact analysis, and long-term stability studies in real food systems.

For industrial adoption, further work is required to optimize pilot-scale electrospinning processes, ensure batch-to-batch reproducibility, and develop cost-effective manufacturing strategies compatible with existing packaging technologies. Integration with smart and connected packaging platforms may further enhance functionality, enabling data-driven quality monitoring aligned with emerging intelligent manufacturing paradigms. Overall, with continued development and regulatory validation, the proposed nanofiber-based colorimetric system holds strong potential as a safe, responsive, and scalable solution for intelligent oil quality monitoring in food packaging applications.

Data availability

The original contributions presented in the study are included in the article/supplementary material; further inquiries can be directed to the corresponding author/s.

Received: 24 November 2025; Accepted: 17 February 2026
Published online: 21 March 2026

References

1. Hashim, A. F., Abd-Rabou, A. A. & El-Sayed, H. S. Functional nanoemulsion and nanocomposite microparticles as an anticolorectal cancer and antimicrobial agent: applied in yogurt. *Biomass Convers. Biorefinery*. **14** (12), 13233–13249 (2024).
2. Akl, E. M., Abd-Rabou, A. A. & Hashim, A. F. Anti-colorectal cancer activity of constructed oleogels based on encapsulated bioactive canola extract in lecithin for edible semisolid applications. *Sci. Rep.* **15** (1), 4945 (2025).
3. El-Sayed, S. M. & Hashim, A. F. Development of emulsion foams based on healthier oleogels and their application as low-fat replacers for whipped cream. *J. Food Meas. Charact.* **18** (11), 9142–9155 (2024).
4. Mahmoud, M. Y., Altamim, E. A. & Zahran, H. A. Natural Antioxidants from Dehydrated Orange (Citrus sinensis L.) Peels: A Novel Approach to Mitigate Carcinogenic Substances in Used Cooking Oil. *Egypt. J. Chem.* **67** (13), 1813–1822 (2024).
5. Reis, F., Wu, S. & Potyatynnyk, K. Life in plastic, it's not fantastic: the economics of plastic pollution. *Sci. Sustain. (S4S) J.* **1**(1), 1–9 (2017).
6. Abedi-Firoozjah, R. et al. *Alginate-based edible films/coatings/nanofibers in food packaging: A comprehensive review of recent advances* 100955 (Carbohydrate Polymer Technologies and Applications, 2025).
7. Alghuthaymi, M. A., Ali, A. A., Hashim, A. F. & Abd-Elsalam, K. A. A rapid method for the detection of Ralstonia solanacearum by isolation DNA from infested potato tubers based on magnetic nanotools. *Philippine Agric. Sci.* **99**, 113–118 (2016).
8. Ahmadi, M. T., Ismail, R. & Anwar, S. (eds) *Handbook of research on nanoelectronic sensor modeling and applications* (IGI Global, 2016).
9. Sheikh-Mohseni, M. A. & Pirsa, S. Nanostructured conducting polymer/copper oxide as a modifier for fabrication of L-DOPA and uric acid electrochemical sensor. *Electroanalysis* **28** (9), 2075–2080 (2016).
10. Pirsa, S. & Alizadeh, N. Rapid determination of pyridine derivatives by dispersive liquid–liquid microextraction coupled with gas chromatography/gas sensor based on nanostructured conducting polypyrrole. *Talanta* **87**, 249–254 (2011a).
11. Jurić, M., Donsì, F., Bandić, L. M. & Jurić, S. Natural-based electrospun nanofibers: Challenges and potential applications in agri-food sector. *Food bioscience*. **56**, 103372 (2023).
12. Gao, X. et al. Strengthening polyacrylonitrile-based carbon nanofibers via a hydrolysis-induced low-energy-barrier cyclization reaction. *Polymer* **317**, 127930 (2025).
13. Abo-Elwafa, G. A., Hashim, A. F., Afifi, S. M., Ahmed, M. & Youssef, A. M. Simplified visual colorimetric method for edible oil oxidation detection using Agarose-Polyvinyl alcohol (AGR/PVA) colorimetric biofilms. *J. Food Meas. Charact.* **20**, 1–17 (2025).
14. Hashim, A. F., Hamed, S. F., Zahran, H. A. & Youssef, A. M. Colorimetric biocomposite sensor using polyvinyl alcohol/sodium alginate film for visual detection of edible oil deterioration. *Food. Anal. Methods*. **18** (9), 2076–2087 (2025a).
15. Xie, M., Jia, M., Zhao, H. & Zhang, L. Visual determination of oxidation of edible oil by a nanofiber mat prepared from polyvinyl alcohol and Schiff's reagent. *Microchim. Acta*. **187**, 1–9 (2020).
16. Liu, X. et al. Visual detection of edible oil oxidation by using chitin-based colorimetric sensor for aldehydes. *Colloids Surf., A*. **628**, 127303 (2021).
17. Hashim, A. F., Abo-Elwafa, G. A., Ibrahim, S. M. & Hamouda, T. Fast visual detection of sunflower oil thermal oxidation using Polyacrylonitrile/Congo red nanofiber mats. *Food Chem.* **472**, 142961 (2025).

18. Chen, W. A., Chiu, C. P., Cheng, W. C., Hsu, C. K. & Kuo, M. I. Total polar compounds and acid values of repeatedly used frying oils measured by standard and rapid methods. *J. Food Drug Anal.* **21** (1), 3 (2013).
19. Srivastava, G. K. et al. Comparison between direct contact and extract exposure methods for PFO cytotoxicity evaluation. *Sci. Rep.* **8** (1), 1425 (2018).
20. Li, X., Zhu, H., Shoemaker, C. F. & Wang, S. C. The effect of different cold storage conditions on the compositions of extra virgin olive oil. *J. Am. Oil Chem. Soc.* **91**, 1559–1570 (2014).
21. Salahuddin, N., Elbarbary, A., Allam, N. G. & Hashim, A. F. Polyamide-montmorillonite nanocomposites as a drug delivery system: Preparation, release of 1, 3, 4-oxa (thia) diazoles, and antimicrobial activity. *J. Appl. Polym. Sci.* **131**(23), 1–14 (2014).
22. Moon, S. A., Salunke, B. K., Saha, P., Deshmukh, A. R. & Kim, B. S. Comparison of dye degradation potential of biosynthesized copper oxide, manganese dioxide, and silver nanoparticles using Kalopanax pictus plant extract. *Korean J. Chem. Eng.* **35**, 702–708 (2018).
23. Yildiz, A. Y., Öztekin, S. & Anaya, K. Effects of plant-derived antioxidants to the oxidative stability of edible oils under thermal and storage conditions: Benefits, challenges and sustainable solutions. *Food Chem.* **479**, 143752 (2025).
24. Bahramian, B. et al. Multifunctional performance of gallic acid in biodegradable food packaging films and coatings: Mechanisms, developments, applications, and horizons. *Eur. Polymer J.* **221**, 113559 (2024).
25. El-Sayed, H. S., Youssef, K. & Hashim, A. F. Stirred yogurt as a delivery matrix for freeze-dried microcapsules of synbiotic EVOO nanoemulsion and nanocomposite. *Front. Microbiol.* **13**, 893053 (2022).
26. Guo, Y. et al. Effects of refining process on Camellia vietnamensis oil: Phytochemical composition, antioxidant capacity, and anti-inflammatory activity in THP-1 macrophages. *Food Bioscience*. **52**, 102440Y (2023).
27. Rękas, A., Wroniak, M. & Krygier, K. Effects of different roasting conditions on the nutritional value and oxidative stability of high-oleic and yellow-seeded Brassica napus oils. *Grasas y Aceites*. **66** (3), e092–e092 (2015).
28. International Olive Council (IOC). (2016). http://www.internationaloliveoil.org/estaticos/view/131-world-olive-oil-figures Accessed 17th May 2017.
29. International Olive Council. (IOC)Trade standard applying to olive oils and olive-pomace oils. COI/T.15/NC No. *3/Rev* **11** (2016).
30. Ceci, L. N., Mattar, S. B. & Carelli, A. A. Chemical quality and oxidative stability of extra virgin olive oils from San Juan province (Argentina). *Food Res. Int.* **100**, 764–770 (2017).
31. Esfahani, S. T., Zamindar, N., Esmaeili, Y. & Sharifian, S. Effect of initial quality of oil and thermal processing on oxidation indexes in canned tuna. *Appl. Food Res.* **4** (2), 100553 (2024).
32. Alizadeh, N., Ataei, A. A. & Pirsa, S. Nanostructured conducting polypyrrole film prepared by chemical vapor deposition on the interdigital electrodes at room temperature under atmospheric condition and its application as gas sensor. *J. Iran. Chem. Soc.* **12** (9), 1585–1594 (2015b).
33. Alizadeh, N., Pirsa, S., Mani-Varnosfaderani, A. & Alizadeh, M. S. Design and fabrication of open-tubular array gas sensors based on conducting polypyrrole modified with crown ethers for simultaneous determination of alkylamines. *IEEE Sens. J.* **15** (7), 4130–4136 (2015a).
34. Pirsa, S. & Alizadeh, N. Nanoporous conducting polypyrrole gas sensor coupled to a gas chromatograph for determination of aromatic hydrocarbons using dispersive liquid–liquid microextraction method. *IEEE Sens. J.* **11** (12), 3400–3405 (2011b).
35. Pirsa, S., Heidari, H. & Lotfi, J. Design selective gas sensors based on nano-sized polypyrrole/polytetrafluoroethylene and polypropylene membranes. *IEEE Sens. J.* **16** (9), 2922–2928 (2016).
36. Xu, L., Yu, X., Li, M., Chen, J. & Wang, X. Monitoring oxidative stability and changes in key volatile compounds in edible oils during ambient storage through HS-SPME/GC–MS. *Int. J. Food Prop.* **20** (sup3), S2926–S2938 (2017).
37. Bahramian, B., et al. Biodegradable active packaging films based on methyl cellulose/chitosan nanofibers and turnip peel carbon dots for perishable food preservation. *Carbohydrate Polymer Technologies and Applications,* 100950 (2025).
38. Manzoor, S., et al. Sustainable development goals through reducing food loss and food waste: A comprehensive review. *Future Foods,* **9**, 100362 (2024)..
39. Ma, L. et al. (ed, Q.) The effect of heating on the formation of 4-hydroxy-2-hexenal and 4-hydroxy-2-nonenal in unsaturated vegetable oils: Evaluation of oxidation indicators. *Food Chem.* **321** 126603 (2020).
40. Lanza, B. & Ninfali, P. Antioxidants in extra virgin olive oil and table olives: Connections between agriculture and processing for health choices. *Antioxidants* **9** (1), 41 (2020).
41. Ayala, A., Muñoz, M. F. & Argüelles, S. Lipid peroxidation: production, metabolism, and signaling mechanisms of malondialdehyde and 4-hydroxy-2-nonenal. *Oxidative Med. Cell. Longev.* **2014** (1), 360438 (2014).
42. Ibrahim, S., Ahmad, A. & Mohamed, N. S. Characterization of novel castor oil-based polyurethane polymer electrolytes. *Polymers* **7** (4), 747–759 (2015).
43. Soliman, H. M. & Zahran, H. A. Synthesis of a new hydrophobic coating film from stearic acid of buffalo fat. *Sci. Rep.* **12** (1), 18465 (2022).
44. Al Amin, M., Ali, M. A., Alam, M. S., Nahar, A. & Chew, S. C. Oxidative degradation of sunflower oil blended with roasted sesame oil during heating at frying temperature. *Grain Oil Sci. Technol.* **6** (1), 34–42 (2023).
45. Poiana, M. A. et al. Use of ATR-FTIR spectroscopy to detect the changes in extra virgin olive oil by adulteration with soybean oil and high temperature heat treatment. *Open. Chem.* **13** (1), 000010151520150110 (2015).
46. Dodoo, D. et al. Quality evaluation of different repeatedly heated vegetable oils for deep-frying of yam fries. *Measurement: Food.* **7**, 100035 (2022).
47. Xu, L., Yu, X., Liu, L. & Zhang, R. A novel method for qualitative analysis of edible oil oxidation using an electronic nose. *Food Chem.* **202**, 229–235 (2016).
48. Jimenez-Lopez, C., et al. Bioactive compounds and quality of extra virgin olive oil. *Foods*, **9**(8), 1014 (2020).
49. De Meyer, T. et al. Halochromic properties of sulfonphthaleine dyes in a textile environment: The influence of substituents. *Dyes Pigm.* **124**, 249–257 (2016).
50. Khanjanzadeh, H. & Park, B. D. Covalent immobilization of bromocresol purple on cellulose nanocrystals for use in pH-responsive indicator films. *Carbohydr. Polym.* **273**, 118550 (2021).
51. Yao, Y. et al. Modification of Polyacrylonitrile Fibers by Coupling to Thiosemicarbazones. *Materials* **12** (23), 3980 (2019).
52. Ishak, S. A. et al. The application of modified natural polymers in toxicant dye compounds wastewater: A review. *Water* **12** (7), 2032 (2020).
53. Lambré, C. et al. Safety assessment of the substance chopped carbon fibres, from carbonised polyacrylonitrile, for use in food contact materials. *EFSA J.* **20** (1), e07003 (2022).

Author contributions

A. F. H.: Conceptualization, methodology, investigation, data curation, formal analysis, software, writing – original draft preparation. H. A. Z.: Methodology, resources, validation, writing, review, and editing. S. M. A.: Methodology, Investigation, visualization, data analysis. A. A. A.: Methodology, Investigation, visualization, data analysis, writing – original draft preparation. S. F. H.: validation, writing, review and editing.

Funding
Open access funding provided by The Science, Technology & Innovation Funding Authority (STDF) in cooperation with The Egyptian Knowledge Bank (EKB). This research was supported by the National Research Centre, Egypt, through project number 13050303.

Declarations

Competing interests
The authors declare no competing interests.

Additional information
Correspondence and requests for materials should be addressed to A.F.H.

Reprints and permissions information is available at www.nature.com/reprints.

Publisher's note Springer Nature remains neutral with regard to jurisdictional claims in published maps and institutional affiliations.